Molecular Structures, Energetics, and Electronic Properties of Neutral and Charged Hg_n Clusters ($n = 2-8$)

Jeewon Kang,[†] Joonghan Kim,[‡] Hyotcherl Ihee,[‡] and Yoon Sup Lee*,[†]

Department of Chemistry, KAIST, Daejeon, 305-701, Republic of Korea, and Center for Time-Resolved Diffraction, Department of Chemistry, Graduate School of Nanoscience & Technology (WCU), KAIST, Daejeon, 305-701, Republic of Korea

Received: October 10, 2009; Revised Manuscript Received: February 17, 2010

The geometric and electronic structures of small mercury clusters, Hg_n, Hg_n^+, and Hg_n^- ($n \leq 8$) have been calculated using a density functional theory. The results indicate that as the cluster size increases, the lowest energy states of neutral and anionic mercury clusters prefer three-dimensional structure whereas those of cationic clusters are peculiarly linear structure due to *s-p* hybridization. This structural feature has influence on the energetic and electronic properties of cationic clusters which deviate from the characteristics of van der Waals cluster. As the cluster size increases, energetic properties, binding energies per atom and second order difference in total energy of cationic clusters consistently decrease, in contrast to the neutral and anionic clusters. However, neutral and charged mercury clusters show common features in terms of size dependent transition of bonding character, such as the decrease of band gap and vertical ionization potential, and the increase of vertical electron affinity. These various properties are also qualitatively and quantitatively in line with the available experimental and theoretical results, implying the reliability of the ground state geometries of these clusters.

I. Introduction

Size-dependent characteristics of divalent metal clusters, especially mercury clusters, have received particular attentions due to the change of bonding character from van der Waals (vdW) to covalent to metallic bonding as the cluster size increases. During the last two decades, many experimental and theoretical studies have focused on these size-dependent properties of mercury clusters, especially transition point of bonding characters. Brechignac et al.[1] recorded the core−valence autoionization lines (5d → 6p) of mercury clusters, Hg_n ($n \leq 8$). They extended these size-dependence studies[2] up to $n = 40$ and found that the transition from vdW to metallic binding occurs in the size range of $n = 13-20$. Rademann et al.[3] measured the ionization potentials by photoionization photoelectron coincidence technique for $n \leq 70$. Harberland et al.[4] extended it up to $n = 100$ using electron-impact ionization and reported the following trend; vdW bonding: $n \leq 13$, vdW to covalent: $30 \leq n \leq 70$, metallic: $n \geq 100$. These experimental studies were accompanied by theoretical calculations ($n = 13$).[5–7] On the other hand, Busani et al.[8] measured the photoelectron spectra of mass-selected negatively charged mercury clusters Hg_n^- in the size range $n = 3-250$ and suggested the complete band gap closure at the size range of $n = 400 \pm 30$, considerably larger value than previously reported.

Most previous theoretical studies have contributed to the understanding of small and medium size Hg_n ($n < 80$) clusters with effective Hamiltonian methods[7,9] and quantum chemical calculations.[10–16] In addition to these size-dependent properties, Hg_n clusters show dramatic changes in the electronic structure after the ionization process.[17] Like rare-gas clusters,[18,19] charged mercury clusters are good examples of divalent metal systems, which dramatically change their bonding characters upon ionization of the cluster. After the ionization, attractive interactions between the atoms substantially increase by the increase of s−p hybridization, in addition to weak vdW interactions present before ionization. Therefore, one may say that mercury clusters undergo a vdW-to-covalent transition upon ionization. However, very few results are available in the literature for the ionized (cations and anions) Hg_n clusters. To clarify this aspect, we have carried out a systematic study of the structure and energetics of the singly charged (both anionic and cationic) mercury clusters and compared them with those of neutral clusters. In specific, size-dependent electronic and structural properties of mercury clusters were investigated by the density functional theory (DFT) calculation.

Generally, it is difficult to accurately describe the weak bonding properties using quantum chemical calculations, and the relative stability of the structures is very sensitive to the methods applied and the quality of basis sets. Thus, we used a sufficiently large basis set that was recently developed and the hybrid DFT functionals instead of the GGA used in previous theoretical works.[10,12,15] This set gives better results not only in the test calculations but also in the neutral and charged mercury clusters. To the best of our knowledge, this is the most extensive theoretical investigation reported on the ground and low-lying states of the neutral, cationic, and anionic Hg_n ($n \leq 8$) clusters. Although experimental results are available for a rather large range of cluster size, understanding of structural growth behavior in even the small clusters is crucial to elucidate how matter evolves from atoms to solids. In Section II we briefly present some technical details of the method and the theory level employed. Section III.A describes the cluster structures obtained in this work and compare them to previous theoretical results. Sections III.B and III.C show a comparison with experimental

* To whom correspondence should be addressed. E-mail: yslee@kaist.edu.
[†] Department of Chemistry, KAIST.
[‡] Center for Time-Resolved Diffraction, Department of Chemistry, Graduate School of Nanoscience & Technology (WCU), KAIST.

10.1021/jp909703u
Published on Web 04/19/2010

results regarding cluster stability, structural, and electronic properties. Finally, in Section IV we briefly summarize our main conclusions.

II. Computational Details

The geometries and harmonic vibrational frequencies were calculated using DFT with the PBE0[20–22] (25% of exact exchange energy) exchange-correlation functional and the small core energy-consistent pseudopotential (PP) for Hg.[23] The aug-cc-pVTZ level basis set was used for valence electrons ((11s10p9d3f2g)/[6s6p5d3f2g]).[24] We refer to this combination as the aug-cc-pVTZ-PP. All calculations were carried out using the Gaussian 03 program.[25]

Test calculations have been carried out to investigate the effects of the basis sets and exchange-correlation functionals on the mercury dimer. In Table S1 in the Supporting Information, we summarize the results obtained using various functional and basis set schemes. We used LDA,[26] PW91,[27,28] PBE,[29,30] mPWPW91,[31] B3LYP,[32,33] PBE0,[20–22] and mPW1PW91[31] functionals and aug-cc-pVXZ-PP (X = T, Q, and 5), aug-cc-pwCTZ-PP (including the effect of the core-polarization) basis sets. The NWChem 5.1 program[34] was used for M06[35] and M06-L[36] functionals. The geometries and electronic properties are quite sensitive to the kind of the exchange-correlation functional.

Among the tested functionals, the results of PW91, PBE, and PBE0 are in good agreement with the experimental values. Additionally, in Table 1, we calculated the charged mercury dimer using these three functionals and compare the bond length, binding energy, and vibrational frequency with the result of coupled-cluster with single and double and perturbative triple excitations (CCSD(T)[37]) method. We show the relative accuracy of each functionals using mean absolute error (MAE). Although three functionals give good results for neutral Hg_2, for charged mercury clusters, PBE0 are much better than the other two functionals, PW91 and PBE, especially for the dissociation energy (D_e). As a result, the PBE0/aug-cc-pVTZ-PP method is employed for the mercury clusters of large size. Using this scheme, we calculated a considerable amount of structural isomers of each cluster size n, to find out the lowest-energy structure. We also performed the natural population analysis (NPA) to investigate the bonding and electronic properties of Hg_n clusters.

III. Results and Discussion

A. Geometries. The ground states of neutral and singly charged small mercury clusters are studied. The optimized structures of Hg_n, Hg_n^+, and Hg_n^- ($n \leq 8$) clusters are shown in Figure 1, 2, and 3, respectively. The symmetries, average bond length (R_{avg}), binding energies per atom (E_b/n), and HOMO−LUMO gap (E_g) for the lowest-energy structures of mercury clusters are summarized in Table 2. Significant changes in low-lying energy structures are observed between the neutral and charged clusters.

TABLE 1: Bond Lengths, r_e (Å), Dissociation Energies, D_e (eV), and Vibrational Frequencies, ω_e (cm^{-1}) for Hg_2, Hg_2^+, and Hg_2^- Calculated with Various DFT Methods and CCSD(T)[a]

		PW91	PBE	PBE0	CCSD(T)
Hg_2	r_e (Å)	3.526	3.562	3.626	3.737
	ω_e (cm^{-1})	28.2	26.1	18.9	20.14
	D_e (eV)	0.047	0.038	0.029	0.060
Hg_2^+	r_e (Å)	2.807	2.813	2.783	2.721
	ω_e (cm^{-1})	93.1	92.2	99.0	117.4
	D_e (eV)	1.807	1.786	1.667	1.552
Hg_2^-	r_e (Å)	3.514	3.223	3.492	3.357
	ω_e (cm^{-1})	32.1	43.1	31.8	36.25
	D_e (eV)	0.282	0.302	0.222	0.211
MAE (r_e)		0.151	0.133	0.103	
MAE (ω_e)		12.17	12.67	8.03	
MAE (D_e)		0.113	0.096	0.033	
MAE		12.43	12.90	8.16	

[a] Mean absolute errors (MAE) are also shown.

For Hg_2^+, the interatomic separation between Hg atoms decreases from 3.626 to 2.783 Å (3.0 Å for the bulk Hg)[38] after removal of an electron from Hg_2. Overall, average bond length (R_{avg}) of the cationic cluster is about 0.7 Å shorter than that of the neutral cluster. This dramatic structural change is largely due to the increasing covalent bonding character and polarization interaction by positive charge, as the case of the rare-gas cationic clusters such as Xe_n^+, Kr_n^+.[9,15] Our predicted bond length in cationic mercury dimer, Hg_2^+, (2.721 Å, see Table 1) agrees well with the CCSD(T) results of Dolg et al. (2.740 Å),[10] In the case of Hg_2^-, bond length contraction is much smaller than the Hg_2^+, 3.492 Å. For the whole size of anionic cluster, there are slight bond contraction in the range of 0.06−0.25 Å, not as much as cationic system. However, Hg_n^- is also tightly bound compared with neutral Hg_n due to charge-induced-dipole interactions.[11] From molecular orbital (MO) analysis, this bond length contraction is explained by the excess electron occupying p-type bonding orbital, in contrast to the cationic cluster that loses a valence electron from the sigma antibonding orbital.

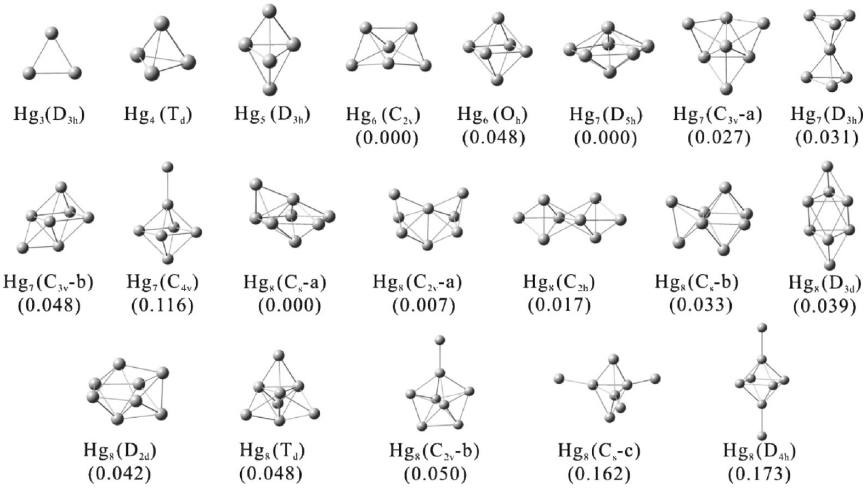

Figure 1. Low-lying isomers of Hg_n ($n = 3-8$) neutral clusters in the order of increasing size and energy (in eV). The relative stabilities of each isomer have been expressed in terms of the difference in total energy with respect to the lowest energy isomer.

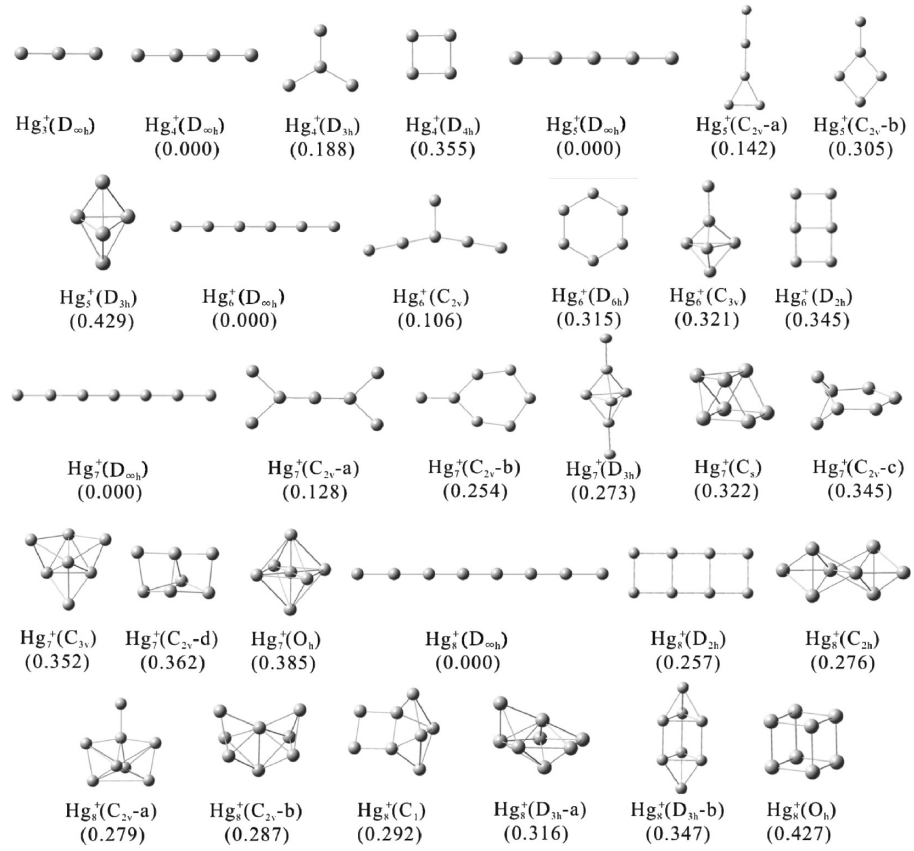

Figure 2. Low-lying isomers of Hg_n^+ ($n = 3-8$) cationic clusters in the order of increasing size and energy (in eV). The relative stabilities of each isomer have been expressed in terms of the difference in total energy with respect to the lowest energy isomer.

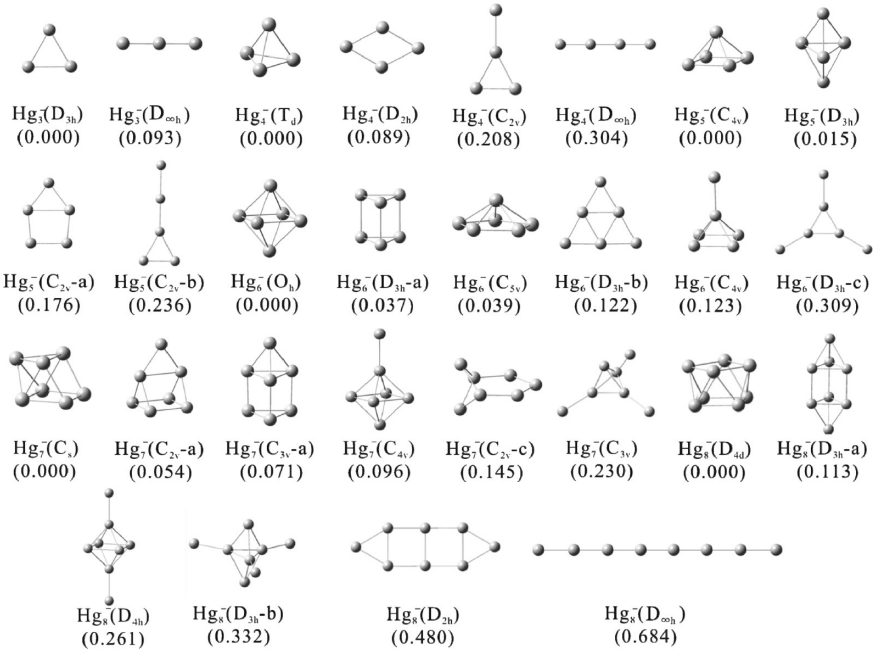

Figure 3. Low-lying isomers of Hg_n^- ($n = 3-8$) anionic clusters in the order of increasing size and energy (in eV). The relative stabilities of each isomer have been expressed in terms of the difference in total energy with respect to the lowest energy isomer.

From Hg_3 to Hg_7, the lowest energy structures are in excellent agreement with previous calculation results of Dolg et al. (CCSD(T) method)[10] and Wang et al. (hybrid model (HM) method).[12,13] Dolg et al. optimized some selected, mostly highly symmetric structures with the CCSD(T) method. They extended to negatively charged structures for $n = 5-7$ by simply adding an excess electron to the structure of neutral cluster and then reoptimized it under the assumption of neutral and negatively charged mercury clusters have similar structures. On the other hand, we have explored massive structural isomers and optimized using the DFT method. Therefore, in this work, we have found considerable number of new stable isomers for neutral and charged mercury clusters that have not been reported before. Moreover, systematic structural analysis of anionic clusters is performed for the first time.

TABLE 2: DFT Calculation Data for the Most Stable Structures of Hg_n, Hg_n^+, and Hg_n^- ($n = 3-8$) Clusters Using PBE0 Functional (PBE0/aug-cc-pVTZ-PP); Average Bond Length, R_{avg} (Å); Binding Energies Per Atom, E_b/n (eV); and the HOMO−LUMO Gap, E_g (eV)

n	symmetry	R_{avg} (Å)	E_b (eV)	E_b/n (eV)	E_g (eV)
			Hg_n		
3	D_{3h}	3.547	0.092	0.031	5.742
4	T_d	3.437	0.219	0.055	5.469
5	D_{3h}	3.504	0.302	0.060	5.061
6	C_{2v}	3.506	0.387	0.065	5.089
7	D_{5h}	3.588	0.495	0.071	5.007
8	C_s	3.541	0.593	0.074	4.898
			Hg_n^+		
3	$D_{\infty h}$	2.816	2.540	0.847	1.806
4	$D_{\infty h}$	2.845	3.086	0.771	1.545
5	$D_{\infty h}$	2.871	3.455	0.691	1.363
6	$D_{\infty h}$	2.894	3.720	0.620	1.230
7	$D_{\infty h}$	2.917	3.918	0.560	1.130
8	$D_{\infty h}$	2.940	4.070	0.509	1.052
			Hg_n^-		
3	D_{3h}	3.353	0.592	0.197	1.013
4	T_d	3.294	1.022	0.256	1.176
5	C_{4v}	3.344	1.246	0.249	1.175
6	O_h	3.439	1.518	0.253	1.143
7	C_s	3.370	1.745	0.249	1.165
8	D_{4d}	3.295	2.037	0.255	1.123

For Hg_3, an equilateral triangle (D_{3h}) is the most stable structure of the neutral cluster (R_{avg}: 3.547 Å). Dolg et al. initially assumed D_{3h} structure and optimized with CCSD(T) method (R_{avg}: 3.514 Å).[10] We also obtained the D_{3h} as the most stable structure of the anionic Hg_3 cluster (R_{avg}: 3.353 Å). The next higher energy isomer of Hg_3^- is linear (0.093 eV) with the bond length of 3.489 Å. Upon removal of an electron, Hg_3^+ favors a linear structure ($D_{\infty h}$) with the bond length of 2.816 Å. This preference of linear structure for the cationic mercury cluster, Hg_n^+, is observed until n reaches 8, in contrast to the DFT ($n = 6$) and MP2 ($n = 5$) calculation results of Gaston et al.[15] The lowest energy structure of both Hg_4 and Hg_4^- clusters are tetrahedron (T_d), and the average bond length is 3.437 Å (CCSD(T) R_{avg}: 3.350 Å) and 3.294 Å, respectively. The next higher energy isomers of Hg_4^- are a diamond structure with the D_{2h} (0.089 eV) symmetry, a capped equilateral triangle structure with C_{2v} (0.208 eV) symmetry, and a linear structure (0.304 eV). For Hg_4^+, a linear form ($D_{\infty h}$) is the most stable and the other two planar structures for Hg_4^+ lie 0.188 eV (D_{3h}) and 0.355 eV (D_{4h}) above in energy. Among them, Gaston et al.[15] obtained linear and D_{3h} structure as a local minimum.

From the size five, we have many local minimum structures for anionic and cationic clusters (see Figure 2 and 3). For Hg_5, the lowest energy structure we found is a trigonal bipyramidal (D_{3h}) with the average bond length of 3.504 Å comparable with the value of 3.343 Å calculated by CCSD(T) method.[10,16] Trigonal bipyramidal is also a local minimum of Hg_5^-, but a pyramid (C_{4v}) structure is slightly more stable by 0.015 eV. However, in a previous HM study,[12] D_{3h} is more stable than the C_{4v} structure, and even the energy difference is only 0.05 eV. Additionally, we obtained two planar isomers, one with C_{2v}-*a* and the other with C_{2v}-*b* symmetry, at energies higher by 0.176 and 0.236 eV, respectively. For Hg_5^+, the lowest energy structure is linear ($D_{\infty h}$) with the average bond length of 2.871 Å. The C_{2v}-*a* and C_{2v}-*b* symmetry planar isomers are 0.142 and 0.305 eV less stable than the linear structure. In contrast to the neutral case, the trigonal bipyramidal (D_{3h}) structure is 0.429 eV higher in energy compared to the lowest energy state. All these cationic local minimum structures coincide with previous MP2 and DFT calculation results.[15] The ground state structure of Hg_6 cluster is a bicapped tetrahedral with the C_{2v} symmetry, which is energetically more stable than the octahedron (O_h) structure by 0.048 eV. Wang et al. also obtained a bicapped tetrahedral for the global minimum structure of neutral Hg_6. After adding one electron to this structure, they compared the energy difference between the above-mentioned C_{2v} and the additionally proposed O_h structures using HM. As a result, the anionic Hg_6^- cluster is found to favor the octahedron (O_h) structure both by Wang et al. and in this study. Two almost degenerate low-lying three-dimensional isomers (Figure 3, Hg_6 (D_{3h}-*a*), Hg_6 (C_{5v})) were obtained for Hg_6^-, which is higher than the ground state structure by 0.037 eV. Two planar D_{3h} and C_{4v} symmetry structures are also obtained at 0.122 and 0.309 eV, respectively, above the ground state. For Hg_6^+, the linear structure is the most stable and C_{2v}, D_{6h}, C_{3v}, and D_{2h} symmetry structures are the next low-lying energy isomers (see Figure 2). C_{2v} and D_{6h} structures are newly proposed local minimum structures of Hg_6^+. The C_{3v} structure is the global minimum for the MP2 calculation, and the linear structure is also preferred by other DFT methods, LDA and GGA (PW91).[15] For Hg_7, a pentagonal bipyramidal (D_{5h}) is preferred by 0.027 eV over the tricapped tetrahedron (C_{3v}-*a*) structure with average bond length of 3.588 Å. Our results agree well with those from previous theoretical calculations,[12,13] which show that D_{5h} is the ground state for Hg_7. Next low-lying energy isomers have D_{3h}, capped-O_h and C_{4v} symmetry (Figure 1). The Hg_7^+ cationic cluster still prefers a linear structure with the average bond length of 2.917 Å, as shown in Figure 2 and Table 2. Two planar structures, C_{2v}-*a* and C_{2v}-*b*, are about 0.128 and 0.254 eV, respectively, less stable than the ground state. We also found that D_{3h}, C_s, C_{2v}-*c*, C_{3v}, C_{2v}-*d*, and O_h structures lie about 0.45 eV above the lowest energy linear structure. For the case of Hg_7^-, geometry optimization of the capped-O_h leads to capped trigonal prism structure with the C_s symmetry. Other two isomers (C_{2v}-*a* and C_{3v}-*a*) for Hg_7^- are also capped trigonal prism structure with different positions of capping atoms and lie 0.054 and 0.071 eV higher in energy than the lowest energy structure, respectively. The next higher energy isomers are C_{3v}-*a*, C_{4v}, C_{2v}-*c*, and C_{3v}. (see Figure 3).

For Hg_8, the lowest energy structure of Hg_8 can be described as a capped pentagonal bipyramidal (C_s-*a*) with the average bond length of 3.353 Å. This result is in line with the previous result of icosahedral growth pattern of mercury clusters.[13] However, Dolg et al.[10] initially assumed the cubic structure and optimized that with the CCSD(T) method (O_h R_{avg}: 3.649 Å). Gaston et al.[16] optimized LJ and Hartke isomers[14] and got various minimum structures depending upon the applied calculation methods, MP2 and DFT. In this work, we have nine more three-dimensional minimum isomers for Hg_8. Some appear in the above-mentioned results, but there are newly optimized ones. For Hg_8^-, Hg_8 (D_{4d}) with the average bond length of 3.295 Å is the lowest-energy structure (Figure 3). This structure can be obtained by capping the opposite side of capped-trigonal prism of Hg_7 (C_s) structure. However, there are no comparable calculation data for Hg_8^-. For Hg_8^+, the linear structure is still the lowest energy isomer with the average bond length of 2.940 Å. This result is different from the previous investigation where 3D Hg_n^+ structures appear from $n = 7$ using DFT (PW91) and MP2 calculations.[15] A planar structure (D_{2h}) for Hg_8^+ was also found at the energy higher by 0.257 eV. Three dimensional

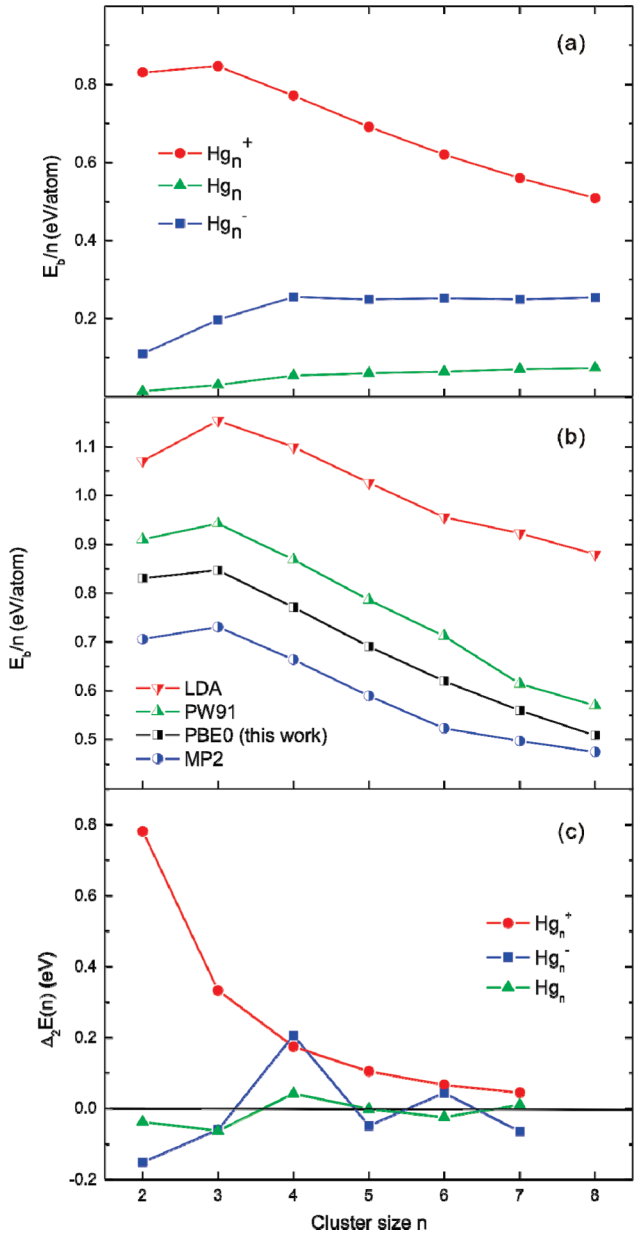

Figure 4. (a) Size dependence of the binding energies per atom (E_b) for both neutral and charged Hg_n clusters (zero-point vibration energy corrected). (b) A comparison of binding energies for cationic clusters with previous calculation results from ref 15. (c) Size dependence of the second energy differences in the total cluster energy [$\Delta_2E(n)$].

isomers, C_{2h}, C_{2v}-*a*, C_{2v}-*b*, C_1, D_{3h}-*a*, D_{3h}-*b*, and O_h with even higher energies, are listed in ascending order of energy (see Figure 2).

For Hg_n, $n = 2-8$, we obtained isomers of neutral and charged mercury clusters that are in line with previously reported calculations and available experimental results. There are considerable changes in the configuration between neutral and charged mercury clusters. Usually, mercury clusters prefer to form 3D compact structures, reflecting the vdW bonding character. However, cationic mercury clusters are found to prefer linear structures up to $n = 8$. We expect that a 2D or 3D structural transition point will exist after $n = 8$ for Hg_n^+. For anionic clusters, we have performed the intensive systematic calculation for the first time.

B. Energies and Relative Stability. To analyze the stability and size-dependent physical properties of mercury clusters, we calculated the binding energies per atom (E_b/n), and second

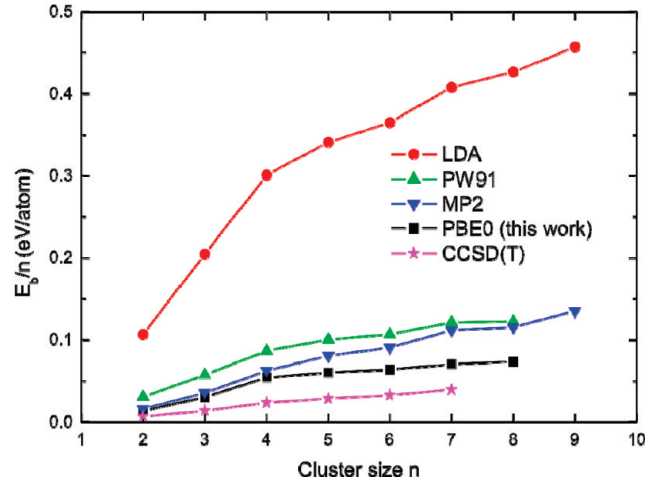

Figure 5. Binding energies per atom (E_b) for neutral clusters compared with the calculation result of LJ isomers from ref 16.

energy differences in total cluster energy [$\Delta_2E(n)$] for the lowest energy isomers (See Figure 4 and 5). Figure 4a represents the average binding energies as a function of cluster size for the neutral and charged mercury Hg_n clusters. The average binding energies, E_b/n (eV), of the neutral, cationic and anionic clusters are calculated as

$$E_b/n(Hg_n) = [nE(Hg) - E(Hg_n)]/n$$

$$E_b/n(Hg_n^+) = [(n-1)E(Hg) + E(Hg^+) - E(Hg_n^+)]/n$$

$$E_b/n(Hg_n^-) = [(n-1)E(Hg) + E(Hg^-) - E(Hg_n^-)]/n$$

repectively, where $E(Hg_n^q, q = -1, 0, +1)$ is the total energy of an *n*-atom cluster.

It is seen that average binding energies of cationic clusters are much higher than the corresponding values of the neutral and anionic counterparts. The positive charge tends to delocalize and at the same time induces polarization of the surrounding neutral atoms, which results in strong attractive interactions between the atoms, in contrast to the weak vdW interactions of neutral clusters.[9] It is interesting that bond lengths between neighboring atoms in the cationic cluster are almost equal and NPA charge is delocalized through the linear cluster in this work (see Figure 6). The equal distribution of the charge indicates that uppermost occupied orbitals are mixed with p-band states. Furthermore, the hybridization of the p-band explains the preference for linear structures of cationic mercury clusters.[15] However, from Table 3, the degree of s−p hybridization of cationic clusters decreases from center to boundary atoms of a linear chain in a symmetric way. These results are correlated with the weakening of charge delocalizations and lengthening of bond lengths in linear cationic mercury clusters Hg_n^+ for large values of *n*. Average binding energy of cationic cluster monotonously decreases from small peak of Hg_3^+ to Hg_8^+ in Figure 4b. This result shows that stabilization energy derived from the linear alignment decreases as the cluster length is elongated. The results of the PBE0 in this work are in qualitatively good agreement with the previous theoretical work by Gaston et al. using MP2 and DFT (LDA, PW91) methods.[15] However, both LDA and MP2 results are poor at describing of binding energies. LDA results are consistently overbinding, and MP2 results are too small. We expect that true binding energy

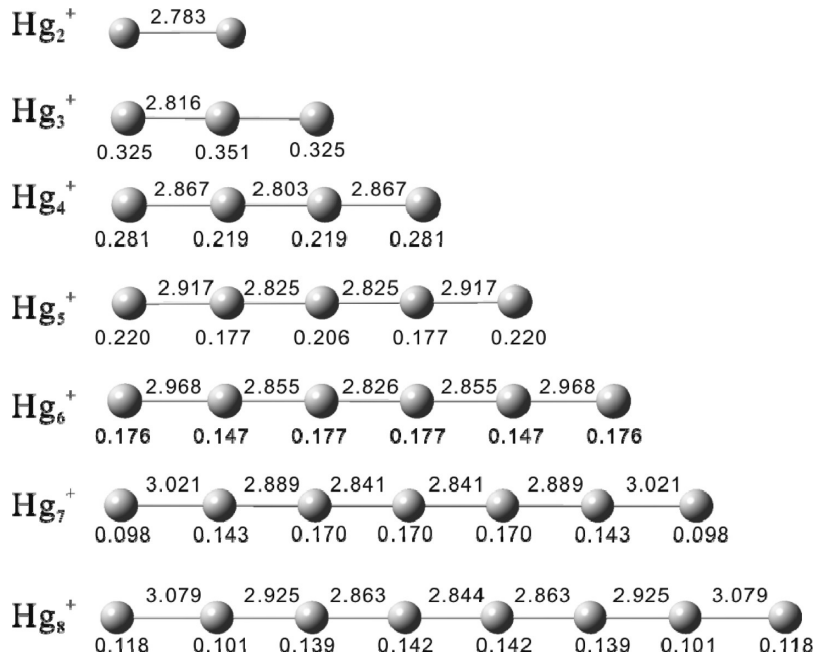

Figure 6. Bond length (in Å) and NPA charge analysis results for cationic mercury clusters. Bond lengths between neighboring atoms are almost equal and NPA charge is delocalized through the linear cluster.

TABLE 3: Natural Electron Occupation Numbers for Cationic Mercury Clusters[a]

	atomic number	6s	5d	6p	7s
Hg_2^+	1	1.48	9.99	0.02	
	2	1.48	9.99	0.02	
Hg_3^+	1	1.65	9.99	0.03	
	2	1.5	9.98	0.06	
	3	1.65	9.99	0.03	
Hg_4^+	1	1.7	9.99	0.03	0.01
	2	1.63	9.98	0.17	
	3	1.63	9.98	0.17	
	4	1.7	9.99	0.03	0.01
Hg_5^+	1	1.76	9.99	0.03	
	2	1.68	9.98	0.16	
	3	1.63	9.98	0.18	
	4	1.68	9.98	0.16	
	5	1.76	9.99	0.03	
Hg_6^+	1	1.8	9.99	0.03	
	2	1.72	9.99	0.15	
	3	1.66	9.98	0.18	
	4	1.66	9.98	0.18	
	5	1.72	9.99	0.15	
	6	1.8	9.99	0.03	
Hg_7^+	1	1.81	9.99	0.05	
	2	1.76	9.99	0.07	0.01
	3	1.74	9.99	0.08	0.01
	4	1.76	9.99	0.07	0.01
	5	1.81	9.99	0.05	
	6	1.89	9.99	0.02	
	7	1.89	9.99	0.02	
Hg_8^+	1	1.87	9.99	0.02	
	2	1.78	9.99	0.12	
	3	1.71	9.98	0.16	
	4	1.68	9.98	0.19	
	5	1.68	9.98	0.19	
	6	1.71	9.98	0.16	
	7	1.78	9.99	0.12	
	8	1.87	9.99	0.02	

[a] This result represents degree of hybridization in linear chain.

will be in between LDA and MP2, and thus PBE0 results satisfy that condition.

Both neutral and anionic clusters show a trend contrary to the cationic cluster for the average binding energy curve; the vdW interaction increases as the number of atoms increases. We compare the binding energy of the neutral cluster with those from the LJ cluster model calculations of the same structures except for Hg_8 (LDA and PW91: D_{2d}, MP2: C_{2v}, see Figure 5).[16] The LDA shows the severe overbinding pattern again. The PW91 and MP2 values are similar to the CCSD(T) ones, but they are still overbinding. Finally, PBE0 shows the best agreement with CCSD(T) results. According to our calculation results, it seems that the hybrid functional, PBE0, yields quite good results for the binding energy of the vdW clusters, suggesting that PBE0 could be a reasonable alternative approach of vdW type cluster calculations.

There are two more small factors that can change the binding energies that we did not consider in this study: the basis set superposition error (BSSE) and the spin−orbit (SO) interaction. BSSE often decreases the dissociation energy of weakly bound systems by more than 50% at the correlated level when standard HF optimized basis sets are used.[39] In order to reduce BSSE, we have used a recently developed correlation consistent basis set. Moreover, BSSE correction may not change the relative ordering of the different isomers.[16] In addition, we expect that the SO effect does not significantly affect the binding energy and the relative ordering. Because the oxidation state of neutral Hg_n cluster is zero, $5d^{10}$ electron occupation is conserved and only 6s orbitals of each Hg atom constitute the valence molecular orbitals. In Hg_n^+ clusters, the singly occupied molecular orbital (SOMO) contains mainly 6s character, too. However, for Hg_n^- clusters, since unpaired electron can partially occupy a p-type orbital, SO effect leads to further stabilization of the negatively charged species. In spite of this, the increased binding energy due to SO interactions would be 1 order of magnitude smaller than the calculated binding energy. Therefore, the SO effect is negligible in all mercury clusters. Moreover, Dolg et al. reports that the SO contributions to binding energies are less than 0.1 eV. We can expect that our results will not change even if these two factors are considered.

The relative stability for a series of clusters can be obtained through the second-order difference in energy (Δ_2E) plot as shown in Figure 4c. Δ_2E is calculate as

$$\Delta_2E(\mathrm{Hg}_n) = [E(\mathrm{Hg}_{n+1}) + E(\mathrm{Hg}_{n-1}) - 2E(\mathrm{Hg}_n)]$$

$$\Delta_2E(\mathrm{Hg}_n^+) = [E(\mathrm{Hg}_{n+1}^+) + E(\mathrm{Hg}_{n-1}^+) - 2E(\mathrm{Hg}_n^+)]$$

$$\Delta_2E(\mathrm{Hg}_n^-) = [E(\mathrm{Hg}_{n+1}^-) + E(\mathrm{Hg}_{n-1}^-) - 2E(\mathrm{Hg}_n^-)]$$

From the above equations, the clusters with positive Δ_2E are relatively more stable than others that have negative Δ_2E value. For the anionic clusters, clear odd−even oscillation exists in the Δ_2E. It is found that even-sized clusters with $n = 4$ and 6 are relatively more stable than their neighbors. For the neutral systems, there is no preference of even- or odd-sized cluster, but a small peak is found at $n = 4$ and 7. Similar to the above average binding energy, cationic clusters show the stability curve pattern different from neutral and anionic clusters. Δ_2E of cationic clusters consistently decreases with increasing cluster size and is positive for all n. From these two cluster stability terms, E_b/n and Δ_2E, we conclude again that the cationic cluster is destabilized as the linear Hg_n^+ chain length is elongated and finally changes into the 3D structures.

We have also calculated the fragmentation energies of neutral and charged clusters for all possible channels, which is defined as

$$E_f(\mathrm{Hg}_n^q) = E(\mathrm{Hg}_n^q) - E(\mathrm{Hg}_p) - E(\mathrm{Hg}_{n-p}^q)$$

where E (Hg_n^q, $q = -1, 0, +1$) is the total energy of an n-atom cluster.

We plot only the lowest energy fragmentation channels as a function of the cluster size as shown in Figure 7. All neutral and charged mercury clusters prefer monomer dissociation as the lowest energy dissociation path. For cationic and anionic clusters, the larger fragment carries the charge, and a neutral mercury atom is one of the decay products. Although photoionization and mass spectrometry experiments[4,40,41] do not reveal any specific preference of dissociation products, experimentally observed monomer evaporation process is supported by our calculation to be the lowest energy fragmentation channel. Garcia et al.[17] have studied the ionization induced ultrafast dynamics of small Hg_n^+ clusters through ensemble calculations and reported that the fragmentation consists mainly in emission of neutral atoms. Overall, the graph shows a trend similar with the curve of the second energy difference in binding energy. Because of monotonously decreasing tendency of the fragmentation energy, we can expect that cationic clusters are easily fragmented as the chain length is elongated. This is in agreement with previous analysis of binding energy curve.

C. Electronic Properties. The electronic properties including highest occupied molecular orbital-lowest unoccupied molecular orbital (HOMO−LUMO) gap (E_g), MO analysis, charge, vertical ionization potentials (E_{IP}), and electron affinities (E_{EA}) are discussed in this section. The HOMO−LUMO gap has been considered to be an important parameter in judging the chemical stability of small clusters as the energy gap (E_g) is proportional to the chemical stability. We have plotted the energy gap of the neutral Hg_n ($n = 2-8$) clusters as shown in Figure 8. A direct comparison of the E_g and the experimental value shows

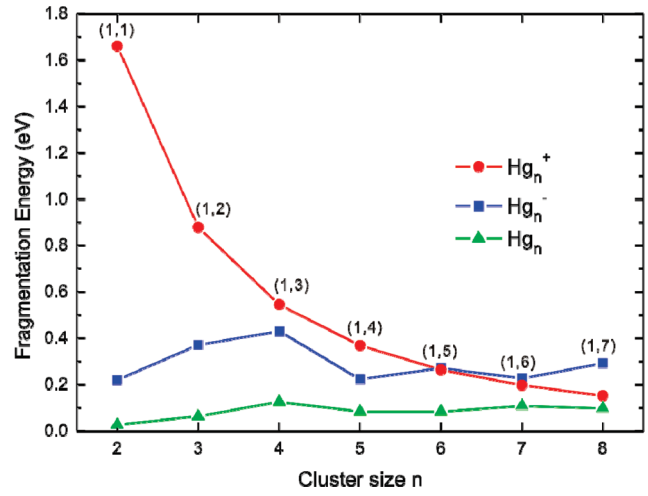

Figure 7. The lowest energy fragmentation channels of Hg_n, Hg_n^+, and Hg_n^- clusters. The numbers in bracket indicate the product fragments (neutral and charged products).

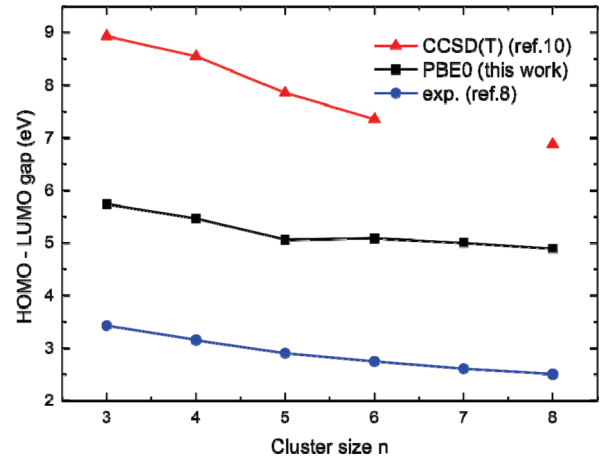

Figure 8. The HOMO−LUMO energy gap (E_g) of mercury clusters as a function of cluster size. CCSD(T) calculation results are taken from Dolg and Flad[10] and the experimental values are from Busani et al.[8]

rather large discrepancies. In this work, although the calculated E_g values are consistently ~2.3 eV larger than the experimental values, the trend of the reduction of HOMO−LUMO gap with the cluster size is reproduced well, which is clearly reflecting a change in bonding characters from vdW toward metallic.[8]

HOMO and LUMO of the lowest-energy configurations of Hg_n, Hg_n^+, and Hg_n^- clusters are shown in Figure 9 and we have performed MO analysis. For the neutral clusters, the HOMO is mainly 6s antibonding type, implying that they are vdW complexes; whereas, LUMO is mainly p atomic orbital mixed with a small amount of s ones. We find that the HOMO of cationic clusters contains s and p characters. The s−p hybridization is probably responsible for the peculiar properties of cationic clusters, namely the preference for the linear structure.[15] Although the LUMO is mainly composed of 6p, amplitude is mainly localized between the bond centers, showing a clear bonding character. For cationic clusters, the loss of electron from antibonding orbital increases the bond strength and result in contraction of the bond length as shown in Section III.A. As was mentioned before, the excess electron occupies the p-type orbital in anionic clusters and the HOMO and LUMO are composed of p electrons as shown in Figure 9.

We performed the natural population analysis (NPA) for the local minimum structures of mercury clusters. This provides

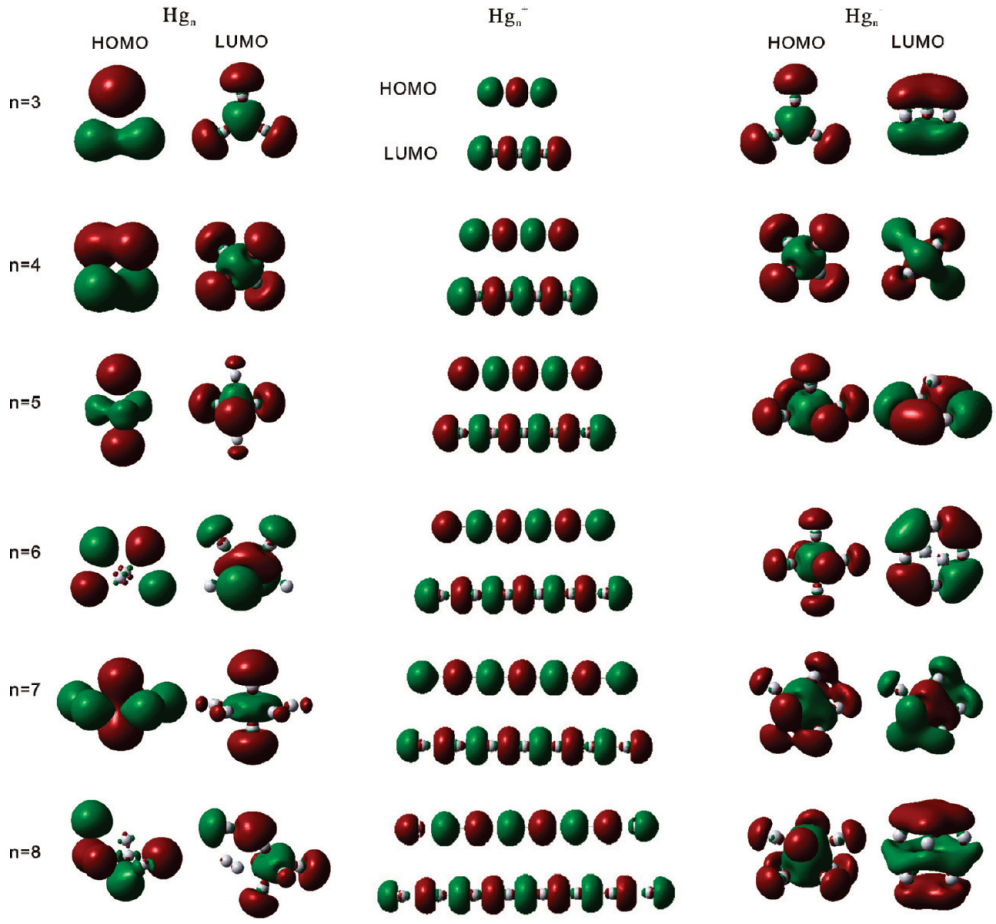

Figure 9. The HOMO and LUMO orbital of Hg_n, Hg_n^+, and Hg_n^- clusters.

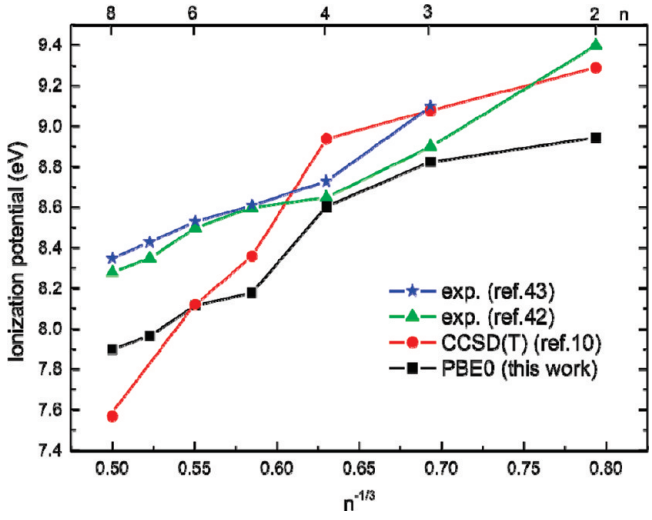

Figure 10. Vertical ionization potentials (E_{IP}) in eV for Hg_n (n = 2−8) clusters in their ground states. Experimental values taken from refs 42 and 43.

clear evidence that s−p hybridizations occur in linear cationic clusters (see Table 3). Furthermore, we have found that charge is perfectly delocalized for anionic 3D structural clusters and cationic linear clusters ($n \leq 6$) as shown in Figure 6. For example, charges are almost equally distributed over the all atoms in Hg_3^+ (0.325, 0.351, 0.325) and Hg_6^+ (0.176, 0.147, 0.177, 0.177, 0.147, 0.176), showing covalent bonding characters. Moreover, bond lengths between neighboring atoms are almost equal. For Hg_3^+, three atoms are equally separated by 2.816 Å and Hg_6^+ shows symmetric structure with r_1 = 2.968 and $r_2 = r_3$ = 2.856 Å. There are large change in the charge distribution and the bond distance depending upon degrees of s−p hybridizations in the linear chain, especially from n = 7. Charge tends to localize near the center, and relatively small amount of charge is located at each end (0.098e, 0.118e). Finally, boundary atoms bonded to the internal clusters with 3.021, 3.079 Å for n = 7 and 8, respectively, clearly approaching the bond length of the metallic bonding character (3.0 Å).[38] From the above results, we expect that the preference for the linear cluster starts to weaken from cationic cluster of size 7. This is in accordance with our previous discussion of 3D transition point, over size 8.

The ionization potential and electron affinity are also important parameters in understanding the trend in electronic stability. We calculated vertical ionization potentials (E_{IP}) and electron affinities (E_{EA}) for the lowest energy isomers as shown in Figure 10 and 11, respectively. The calculated IPs are consistently ~0.4 eV lower than the experimental values.[42,43] Beyond Hg_4, calculated IPs decrease significantly faster than those found in experiment. This discrepancy between this work and experimental studies may be mainly due to the neglect of finite temperature effect in the current investigation since the experimental studies were carried out for hot clusters.[10]

The calculated electron affinities are compared with the experimental value and previous calculation results. Busani et al.[8] measure the binding energy of p-type electron, BE(p), and highest s-type electron, BE(s), of mass-selected negatively charged mercury clusters using photoelectron spectroscopy. BE(p) is matched to the vertical electron affinities (E_{EA}), and BE(s) to the HOMO of the 6s band of the neutral cluster. The

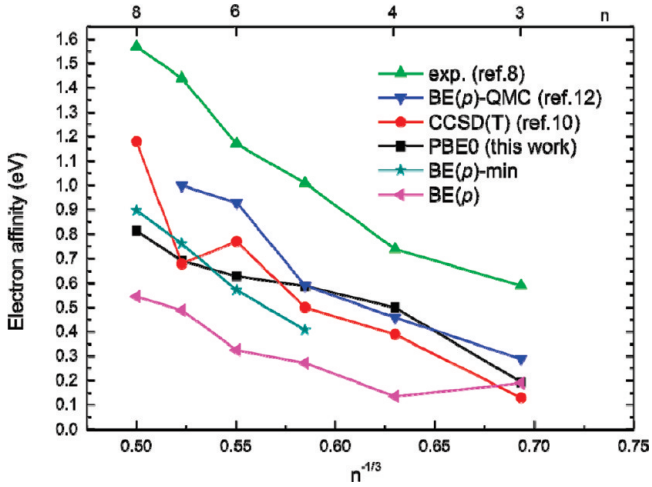

Figure 11. Vertical electron affinity (E_{EA}) in eV for the most stable neutral Hg_n ($n = 2-8$) clusters and binding energies of p-type excess electrons, BE(p), for negatively charged clusters using the structure of neutral cluster. BE(p)-min uses the most stable structure for the anionic clusters. The previous calculation results of CCSD(T) and QMC calculations are taken from refs 10 and 12, and experimental results are from ref 8.

TABLE 4: Calculated Vertical Electron Affinities (E_{EA}) of Hg_n and Binding Energies of p-Type [BE(p)] and s-Type Electrons [BE(s)] for Hg_n^- ($n = 3-8$) Clusters That Have the Lowest Energy Neutral Cluster Structures[a]

n	symmetry	E_{EA}	BE(p)	$BE(p)_{exp}$	BE(s)	$BE(s)_{exp}$
3	D_{3h}	0.19	0.19	0.59	4.79	4.02
4	T_d	0.50	0.14	0.74	4.82	3.9
5	D_{3h}	0.59	0.27	1.01	4.62	3.92
	C_{4v}	0.74	0.41[b]		3.81[c]	
6	C_{2v}	0.63	0.33	1.17	4.60	3.92
	O_h	0.91	0.57[b]		4.00[c]	
7	D_{5h}	0.69	0.49	1.44	4.49	4.05
	C_s	1.13	0.76[b]		4.03[c]	
8	C_s	0.81	0.54	1.57	4.52	4.08
	D_{4d}	1.27	0.90[b]		4.11[c]	

[a] The calculation results are compared with the photoelectron spectroscopy (PES) experimental data of Busani et al.[8] [b] These BE(p) and BE(s) are calculated at the structure of the lowest energy anionic mercury cluster. [c] These BE(p) and BE(s) are calculated at the structure of the lowest energy anionic mercury cluster.

vertical electron affinities (E_{EA}) are calculated by the PBE0 method. For the direct comparison with BE(p) and BE(s) values of Dolg et al.[12] and Busani et al.,[8] we additionally performed single-point calculations of the anionic clusters by the Hartree−Fock (HF) method using the optimized structures of neutral clusters, equilateral triangle (D_{3h}, Hg_3), tetrahedral (T_d, Hg_4), trigonal bipyramidal (D_{3h}, Hg_5), bicapped tetrahedral (C_{2v}, Hg_6), pentagonal bipyramidal (D_{5h}, Hg_7), and capped pentagonal bipyramidal (C_s, Hg_8). The vertical electron affinities (E_{EA}) of neutral clusters (PBE0, black square in Figure 11) and calculated BE(p) values for anionic clusters (HF, BE(p): magenta triangle) are plotted in Figure 11. Although the difference between calculated E_{EA} and experimental values, $BE(p)_{exp}$, are varying from 0.4 eV for Hg_3 to 0.76 eV for Hg_8 (see Table 4), our results well reproduce the overall increasing trend of experimental values with the size of clusters, and are in good agreement with those of the CCSD(T) method. Moreover, BE(p) values differ from the E_{EA} and the $BE(p)_{exp}$ in the range of 0.2−0.4 and 0.4−0.9 eV, respectively. On the basis of our results, from Hg_5 to Hg_8, the neutral and anionic clusters exist in different structures. In order to consider this difference, we extended our calculation of BE(p) using the lowest energy structures of anionic cluster, pyramid (C_{2v}, Hg_5), octahedron (O_h, Hg_6), capped trigonal prism (C_s, Hg_7), and D_{4d} structures (Hg_8), instead of neutral ones, and these are marked as "BE(p)-min" in Figure 11. The BE(p)-min values show better agreement with the experimental ones than the BE(p) ones calculated at the structures of neutral clusters. In addition, we also list the calculated BE(s) with $BE(s)_{exp}$ in Table 4. Like BE(p), the energy difference between BE(s) and $BE(s)_{exp}$ is 0.4−0.9 eV for Hg_3 to Hg_8. The BE(s)-min values show much better agreement with the $BE(s)_{exp}$ values, differing by less than 0.1 eV. These BE(p) and BE(s) results clearly suggest that considering the structural changes in charged clusters is important to obtain reliable electron affinity values.

IV. Conclusions

We have systematically studied the molecular structures, energetics, and electronic properties of neutral and charged mercury clusters. The neutral and anionic clusters show three-dimensional structure as the lowest energy form, whereas the cationic clusters peculiarly prefer the linear structures. Binding energies per atom (E_b/n), second energy differences in total cluster energy [$\Delta_2E(n)$], and fragmentation energies for the lowest energy isomers are investigated. For those energetic properties, cationic clusters show completely different behavior from neutral and negatively charged clusters, reflecting the relation with the structural feature. The stability of the linear structure for the cationic clusters is explained by the s−p hybridization, and the degree of s−p hybridization in a linear cluster affects the charge distribution and bond lengths of the internal chain. Cationic clusters destabilize as the linear chain length is elongated. We have also calculated the lowest energy fragmentation channels for mercury clusters that mainly emit neutral atoms. Due to the change of bonding type from vdW to covalent bond, the HOMO−LUMO gaps for all mercury clusters consistently decrease. The results of NPA suggest that the charge is delocalized for the anionic 3D structural cluster and the cationic linear cluster. All obtained theoretical results are in reasonable agreement with the experimental and previous CCSD(T) calculation results. The present study suggests that, DFT calculation with hybrid functionals (PBE0) could provide reasonable results for the vdW bonding cluster calculation.

Acknowledgment. This work was supported by National Research Foundation of Korea Grant (2009-0076263), funded by the Korean Government, Korea Science and Engineering Foundation Grant (R11-2007-012-03001-0) and the Creative Research Initiatives (Center for Time-Resolved Diffraction) of MEST/NRF. Computational resources were provided by the supercomputing center of the Korea Institute of Science and Technology Information (KISTI). The authors thank Dr. Y. K. Han for a helpful discussion.

Supporting Information Available: Spectroscopic constants such as bond length r_e (Å), binding energies D_e (eV) and vibrational frequencies ω_e (cm^{-1}) of Hg_2 using various DFT functional and basis sets are summarized in Table S1. This material is available free of charge via the Internet at http://pubs.acs.org

References and Notes

(1) Brechignac, C.; Broyer, M.; Cahuzac, P.; Delacretaz, G.; Labastie, P.; Woste, L. *Chem. Phys. Lett.* **1985**, *120*, 559.

(2) Brechignac, C.; Broyer, M.; Cahuzac, P.; Delacretaz, G.; Labastie, P.; Wolf, J. P.; Woste, L. *Phys. Rev. Lett.* **1988**, *60*, 275.
(3) Rademann, K.; Kaiser, B.; Even, U.; Hensel, F. *Phys. Rev. Lett.* **1987**, *59*, 2319.
(4) Haberland, H.; Kornmeier, H.; Langosch, H.; Oschwald, M.; Tanner, G. *J. Chem. Soc. Faraday Trans.* **1990**, *86*, 2473.
(5) Pastor, G. M.; Stampfli, P.; Bennemann, K. H. *Europhys. Lett.* **1988**, *7*, 419.
(6) Pastor, G. M.; Stampfli, P.; Bennemann, K. H. *Z. Phys. D.* **1989**, *12*, 365.
(7) Garcia, M. E.; Pastor, G. M.; Bennemann, K. H. *Phys. Rev. Lett.* **1991**, *67*, 1142.
(8) Busani, R.; Folkers, M.; Cheshnovsky, O. *Phys. Rev. Lett.* **1998**, *81*, 3836.
(9) Garcia, M. E.; Pastor, G. M.; Bennemann, K. H. *Phys. Rev. B* **1993**, *48*, 8388.
(10) Dolg, M.; Flad, H. *Mol. Phys.* **1997**, *91*, 815.
(11) Moyano, G. E.; Wesendrup, R.; Sohnel, T.; Schwerdtfeger, P. *Phys. Rev. Lett.* **2002**, *89*, 103401.
(12) Wang, Y. X.; Flad, H. J.; Dolg, M. *Int. J. Mass Spectrom.* **2000**, *201*, 197.
(13) Wang, Y. X.; Flad, H. J.; Dolg, M. *Phys. Rev. B* **2000**, *61*, 2362.
(14) Hartke, B.; Flad, H. J.; Dolg, M. *Phys. Chem. Chem. Phys.* **2001**, *3*, 5121.
(15) Gaston, N.; Schwerdtfeger, P.; von Issendorff, B. *Phys. Rev. A* **2006**, *74*, 043203.
(16) Gaston, N.; Schwerdtfeger, P. *Phys. Rev. B* **2006**, *74*, 024105.
(17) Garcia, M. E.; Reichardt, D.; Bennemann, K. H. *J. Chem. Phys.* **1998**, *109*, 1101.
(18) Amarouche, M.; Durand, G.; Malrieu, J. P. *J. Chem. Phys.* **1988**, *88*, 1010.
(19) Von Issendorff, B.; Hofmann, A.; Haberland, H. *J. Chem. Phys.* **1999**, *111*, 2513.
(20) Adamo, C.; Barone, V. *Chem. Phys. Lett.* **1998**, *298*, 113.
(21) Ernzerhof, M.; Scuseria, G. E. *J. Chem. Phys.* **1999**, *110*, 5029.
(22) Adamo, C.; Barone, V. *J. Chem. Phys.* **1999**, *110*, 6158.
(23) Figgen, D.; Rauhut, G.; Dolg, M.; Stoll, H. *Chem. Phys.* **2005**, *311*, 227.
(24) Peterson, K. A.; Puzzarini, C. *Theor. Chem. Acc.* **2005**, *114*, 283.
(25) Frisch, R. E., M. J. Trucks, G. W. Schlegel, H. B. Scuseria, G. E. Robb, M. A. Cheeseman, J. R. Montgomery, J. A., Jr., Vreven, T. Kudin, K. N. Burant, J. C. Millam, J. M. Iyengar, S. S. Tomasi, J. Barone, V. Mennucci, B. Cossi, M. Scalmani, G. Rega, N. Petersson, G. A. Nakatsuji, H. Hada, M. Ehara, M. Toyota, K. Fukuda, R. Hasegawa, J. Ishida, M. Nakajima, T. Honda, Y. Kitao, O. Nakai, H. Klene, M. Li, X. Knox, J. E. Hratchian, H. P. Cross, J. B. Bakken, V. Adamo, C. Jaramillo, J. Gomperts, R. Stratmann, R. E. Yazyev, O. Austin, A. J. Cammi, R. Pomelli, C. Ochterski, J. W. Ayala, P. Y. Morokuma, K. Voth, G. A. Salvador, P. Dannenberg, J. J. Zakrzewski, V. G. Dapprich, S. Daniels, A. D. Strain, M. C. Farkas, O. Malick, D. K. Rabuck, A. D. Raghavachari, K. Foresman, J. B. Ortiz, J. V. Cui, Q. Baboul, A. G. Clifford, S. Cioslowski, J. Stefanov, B. B. Liu, G. Liashenko, A. Piskorz, P. Komaromi, I. Martin, R. L. Fox, D. J. Keith, T. Al-Laham, M. A. Peng, C. Y. Nanayakkara, A. Challacombe, M. Gill, P. M. W. Johnson, B. Chen, W. Wong, M. W. Gonzalez, C. Pople, J. A. *Gaussian 03*; Gaussian, Inc.: Wallingford CT, 2004.
(26) MacDonald, A. H.; Vosko, S. H. *J. Phys. C: Solid State Phys.* **1979**, *12*, 2977.
(27) Perdew, J. P.; Chevary, J. A.; Vosko, S. H.; Jackson, K. A.; Pederson, M. R.; Singh, D. J.; Fiolhais, C. *Phys. Rev. B* **1992**, *46*, 6671.
(28) Shi, J. M.; Peeters, F. M.; Hai, G. Q.; Devreese, J. T. *Phys. Rev. B* **1993**, *48*, 4978.
(29) Perdew, J. P.; Burke, K.; Ernzerhof, M. *Phys. Rev. Lett.* **1996**, *77*, 3865.
(30) Perdew, J. P.; Burke, K.; Ernzerhof, M. *Phys. Rev. Lett.* **1997**, *78*, 1396.
(31) Adamo, C.; Barone, V. *J. Chem. Phys.* **1998**, *108*, 664.
(32) Koch, W.; Hertwig, R. H. *Chem. Phys. Lett.* **1997**, *268*, 345.
(33) Stephens, P. J.; Devlin, F. J.; Chabalowski, C. F.; Frisch, M. J. *J. Phys. Chem.* **1994**, *98*, 11623.
(34) Bylaska, E. J. Govind, W. A. d. J., N. Kowalski, K. Straatsma, T. P. Valiev, M. Wang, D. Apra, E. Windus, T. L. Hammond, J. Nichols, P. Hirata, S. Hackler, M. T. Zhao, Y. Fan, P.-D. Harrison, R. J. Dupuis, M. Smith, D. M. A. Nieplocha, J. Tipparaju, V. Krishnan, M. Wu, Q. Van Voorhis, T. Auer, A. A. Nooijen, M. Brown, E. Cisneros, G. Fann, G. I. Fruchtl, H. Garza, J. Hirao, K. Kendall, R. Nichols, J. A. Tsemekhman, K. Wolinski, K. Anchell, J. Bernholdt, D. Borowski, P. Clark, T. Clerc, D. Dachsel, H. Deegan, M. Dyall, K. Elwood, D. Glendening, E. Gutowski, M. Hess, A. Jaffe, J. Johnson, B. Ju, J. Kobayashi, R. Kutteh, R. Lin, Z. Littlefield, R. Long, X. Meng, B. Nakajima, T. Niu, S. Pollack, L. Rosing, M. Sandrone, G. Stave, M. Taylor, H. Thomas, G. van Lenthe, J. Wong, A. Zhang, Z., *NWChem, A Computational Chemistry Package for Parallel Computers, Version 5.1*; Pacific Northwest National Laboratory: Richland, Washington, USA, 2007.
(35) Zhao, Y.; Truhlar, D. G. *Theor. Chem. Acc.* **2008**, *120*, 215.
(36) Zhao, Y.; Truhlar, D. G. *J. Chem. Phys.* **2006**, *125*, 194101.
(37) Raghavachari, K.; Trucks, G. W.; Pople, J. A.; Head-Gordon, M. *Chem. Phys. Lett.* **1989**, *157*, 479.
(38) Lide, D. R. *CRC Handbook of Chemistry and Physics*, 88th ed.; CRC Press: Boca Raton, FL, 2008.
(39) Schwerdtfeger, P.; Wesendrup, R.; Moyano, G. E.; Sadlej, A. J.; Greif, J.; Hensel, F. *J. Chem. Phys.* **2001**, *115*, 7401.
(40) Haberland, H.; Vonissendorff, B.; Ji, Y. F.; Kolar, T.; Thanner, G. *Z. Phys. D* **1993**, *26*, 8.
(41) Blanc, J.; Broyer, M.; Dugourd, P.; Labastie, P.; Sence, M.; Wolf, J. P.; Woste, L. *J. Chem. Phys.* **1995**, *102*, 680.
(42) Cabaud, B.; Hoareau, A.; Melinon, P. *J. Phys. D: Appl. Phys.* **1980**, *13*, 1831.
(43) Busani, R.; Cheshnovsky, O. *J. Phys. Chem. C* **2007**, *111*, 17725.

JP909703U